University of Texas Rio Grande Valley

ScholarWorks @ UTRGV

Electrical and Computer Engineering Faculty Publications and Presentations

College of Engineering and Computer Science

2020

Chlorophyll-Inspired Tunable Metamaterials with Multi-Negative Refractive Index Bands: The Porphyrin Ring and Hydrophobic Tail Effect

Nantakan Wongkasem
The University of Texas Rio Grande Valley

Follow this and additional works at: https://scholarworks.utrgv.edu/ece_fac

Part of the Electrical and Computer Engineering Commons

Recommended Citation

Chlorophyll-Inspired Tunable Metamaterials with Multi-Negative Refractive Index Bands: The Porphyrin Ring and Hydrophobic Tail Effect

Nantakan Wongkasem*

Abstract—Tunable negative electromagnetic properties: permittivity, permeability, and refractive index, in mimic Chlorophyll metamaterial structures in the X- and Ku-band regimes are theoretically and numerically demonstrated. A very broad negative permeability covering the majority of the X- and Ku bands, from 8 GHz to 16 GHz, is observed, while five negative permittivity bands are found within the same range. The two aforementioned properties result in a broad, greater than 25% bandwidth, low-loss negative-refractive index transmission band. These negative electromagnetic properties can be effectively tailored within the low-loss multi-transmission and the high-loss multi-absorption bands in the operating frequency range by modifying the structure's tiller part or the artificial hydrophobic or Phytol tail. By focusing either on the transmission or the absorption bands, these passive always-on bio-inspired metamaterials could be utilized in microelectronic, communication and photonic, and optic devices.

1. INTRODUCTION

Nature is undoubtedly the most astonishing creator in regard to both beauty and functionality. Numerous bio-inspired designs [1–9], also called biomimetics or biomimicry, e.g., arts, structures, architectures, and materials, have been introduced as an innovative strategy translating complexity and diversity principles of function, performance, and aesthetics from biology to human technology and creativity for centuries. Mechanically active dressings to accelerate wound healing were inspired by embryonic wound closure [5]. There was a demonstration indicating that organic and analytical chemistry offer many new strategies and capabilities to problems in long-term, zero-energy, and robust information storage [6]. An overview of the materials used to improve immunotherapies based on artificial cells and artificial microenvironments was presented. The materials were organized based on their characteristic length scale, whereby the enabling feature of each technology was organized by the structure of that material [7]. Endothelial cells representing the first biological barrier for compounds, including nanoparticles, administered *via* the intravascular route has been reported [8]. New biomimetic coatings for passive radiative cooling of objects based on the enhanced optical reflection and radiative heat dissipation found in Saharan silver ants' dense array of triangular hairs could be further developed [9]. Despite substantial research in this field, there are still numerous facets waiting to be exposed, and potentially contribute to a better understanding of the world, leading to boundless mankind benefits.

Metamaterials (MTMs) [10–14] are engineered or manmade materials and structures designed to exhibit unique electromagnetic (EM) and mechanical properties due to their structural repetition. The

performance of MTMs is fundamentally controlled by geometry at multiple length-scales rather than by chemical composition alone. MTMs are excited or stimulated by diverse sources and forces, e.g., electromagnetic fields in photonic MTMs, sound waves in acoustic MTMs, and the flow of heat or diffusive particles in thermodynamic MTMs, respectively. There were several attempts to design bio-inspired MTM structures in a broad EM spectrum ranging from sound wave to the optical frequency [15–21]. It was demonstrated that frustule-inspired hierarchical nanostructure designs could be utilized in broadband infrared metamaterial absorbers [15]. A hierarchical metamaterial for multispectral camouflage of infrared and microwaves was also introduced [16]. Fractal and bio-inspired labyrinthine acoustic metamaterials with non-resonant elements for low-frequency sound control was proposed [17]. By folding the sets of narrow channels into fractal space-filling curves or bio-inspired geometries, one can induce strong artificial Mie-type resonances that allow the achievement of total broadband sound reflection at deep subwavelength scales. Compact acoustic rainbow trapping in a bio-inspired spiral array of graded locally resonant metamaterials were achieved to filter mechanical waves spectrally and spatially to reduce noise and interference in receivers [18]. The effect of bio-inspired hierarchical organization as well as of viscoelasticity on the wave attenuation properties of continuous elastic metamaterials was discussed [19]. Bioinspired multicontrollable metasurfaces and metamaterials for terahertz applications were investigated [20]. A study of bio-inspired nanophotonics on how to manipulate light in nanoscale with plasmonic metamaterials was thoroughly conducted [21].

The question arises: have manmade MTMs' exceptional properties, e.g., negative refractive index (NRI) [12, 22–24], giant optical activity (chirality) [25–30], artificial magnetism [31], acoustic cloaking [32, 33], negative Poisson's ratio [34–36], etc., truly always been part of existing natural compounds? This article focuses on investigating the existence possibility of negative EM property values, i.e., permittivity, permeability, and refractive index, in Chlorophyll, one of the key natural compounds. Chlorophyll, the green photosynthetic pigment found in cyanobacteria and the chloroplasts of algae and plants, was selected because of its remarkable and complex properties and functions. Based on the compound structures and orientation, MTM structures have been designed and optimized in order to tailor and effectively manipulate the aforementioned unique EM properties. Figure 1 exemplifies Chlorophyll compound [37] and an engineered chlorophyll, ChloroGreen, the proposed bio-inspired metamaterials. The ChloroGreen and is designed for theoretical and computational purposes to engage the nature fundamentals and apply the results towards designing close-to-perfect MTMs to reach their maximum EM and photonic performance. The transmission and EM properties from each excitation were numerically demonstrated using full-wave simulations, and then were analyzed based on the structure sizes and orientations. Approximate dimensions of a chlorophyll molecule in a varied millimeter range were modeled to study the properties in the X- and Ku-bands. Note that the proposed structures can be scaled down to the micrometer range to operate in the optical regime taking other optical properties into account.

ChloroGreen has been shown to have well-established low-loss and multi-negative permittivity and ultra-broad permeability transmission bands within the X-and Ku-band operating wavelength. By modifying the ChloroGreen structure, specially the artificial hydrophobic or phytol tail (Figure 2), the

(a)   (b)
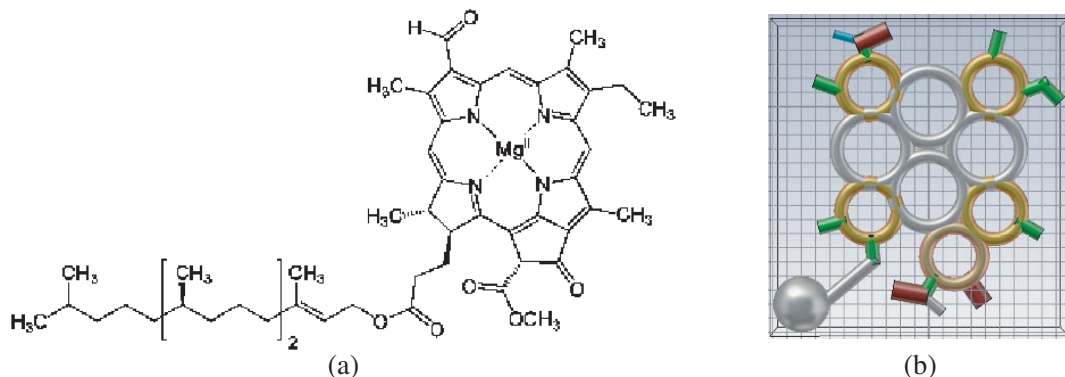
Figure 1. (a) Chlorophyll compound and (b) proposed ChloroGreen metamaterial structure.
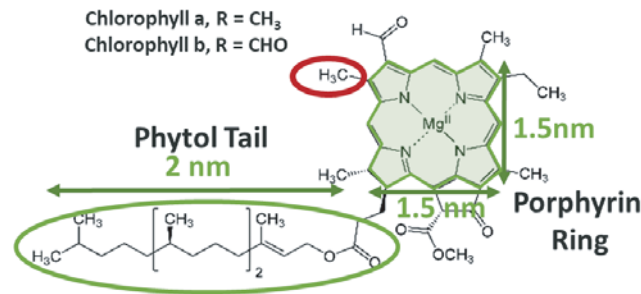
Figure 2. Chlorophyll structure.

negative EM property bands can be effectively tuned. One may also concentrate on high-loss multi absorption bands with negative EM properties in between the transmission bands for other usages. Furthermore, the orientation of the atoms, O and H, and the molecules, CH_3 and CH_3O, indicate the presence of chirality in the ChloroGreen [27–30, 38]. Since one of the NRI transmission bands are greater than 25% bandwidth, this Chlorophyll-inspired MTM design could operate in the broadband spectral domain. These properties are beneficial for antennas, microwave devices, and optoelectronic devices, especially for filters, beamforming and beam steering, and polarization switching applications [27], to name a few.

2. BUILDING UP CHLOROGREEN METAMATERIAL TOWARDS NRI PROPERTY

2.1. Chlorophyll — Multi-Band Light Selector

Chlorophyll [39–41] is the green pigment that absorbs light during photosynthesis. The basic structure of a chlorophyll molecule (Figure 2) is a porphyrin ring, formed around an Magnesium (Mg) central atom, highlighted in green. The ring dimension is approximately $1.5\,\text{nm} \times 1.5\,\text{nm}$. The other main part is a phytol or hydrophobic tail, connected to the bottom left corner of the porphyrin ring. The tail length is around $2\,\text{nm}$ long. There are 2 main types of chlorophyll, named a and b. They differ only slightly, in the composition of a sidechain (in a it is -CH_3, in b it is CHO) [42, 43].

Chlorophyll a, the most important photosynthetic pigment, has the empirical formula $C_{55}H_{72}O_5N_4Mg$. There are also accessory pigments which absorb photons of light that are not absorbed by chlorophyll a and transmit that energy to chlorophyll a.

The most common in plants are chlorophyll b ($C_{55}H_{70}O_6N_4Mg$) and carotenoids [44]. The different side groups in the two chlorophylls 'tune' the absorption spectrum to slightly different wavelengths, so that light that is not significantly absorbed by chlorophyll a at $460\,\text{nm}$, will instead be captured by chlorophyll b, which absorbs strongly at that wavelength. Thus, these two kinds of chlorophyll complement each other in absorbing sunlight [45]. Plants can obtain all their energy requirements from the blue and red parts of the spectrum; however, there is still a large spectral region, between 500–$600\,\text{nm}$, where very little light is absorbed.

On the other hand, this almost absent absorption band can be considered oppositely as a good light transmission range, which is favorable for other applications, e.g., sensors, filters, switching, communications, to name a few. Both the absorption and transmission bands will be investigated while designing the Chlorophyll-inspired metamaterials.

2.2. Building NRI ChloroGreen Metamaterials

Typical one-piece NRI metamaterial structures [46–49] are generally developed based on the combination of a negative permittivity or $(-)\varepsilon$ and a negative permeability or $(-)\mu$. The NRI band is generated from the overlap between a broad $(-)\varepsilon$ band and a magnetic resonance, where the resonance frequency (ω_m) is controlled by the total inductances (L_T) and total capacitances (C_T) of the MTM structure: $\omega_m = 1/\sqrt{L_T C_T}$. The conventional $(-)\varepsilon$ structure is simply an array of straight conductive wires, where the wires must be set parallel to the electric field direction [10], while the standard $(-)\mu$ structure is a

magnetic resonator, where strong magnetic couplings, resulting in $(-)\,\mu$ response, is built between the magnetic field and its broken symmetric ring structure [11]. It was proved that the electric couplings can also create $(-)\,\mu$ [50], but the electric field must be parallel to the broken part or a gap of the structure. In this case, the EM field direction can be set parallel to the structure plane. In order to create multiple NRI bands, a couple broken rings (split ring) of different sizes are required to generate multiple magnetic resonances.

It is important to stress that this ChloroGreen structure was designed to operate within the X- and Ku-band frequency range. Its orientation and parts were adapted and simplified for modelling purposes, as well as the dimensions were not directly scaled down from their actual sizes.

The ChloroGreen was created starting from the porphyrin ring part, considered as a backbone of the
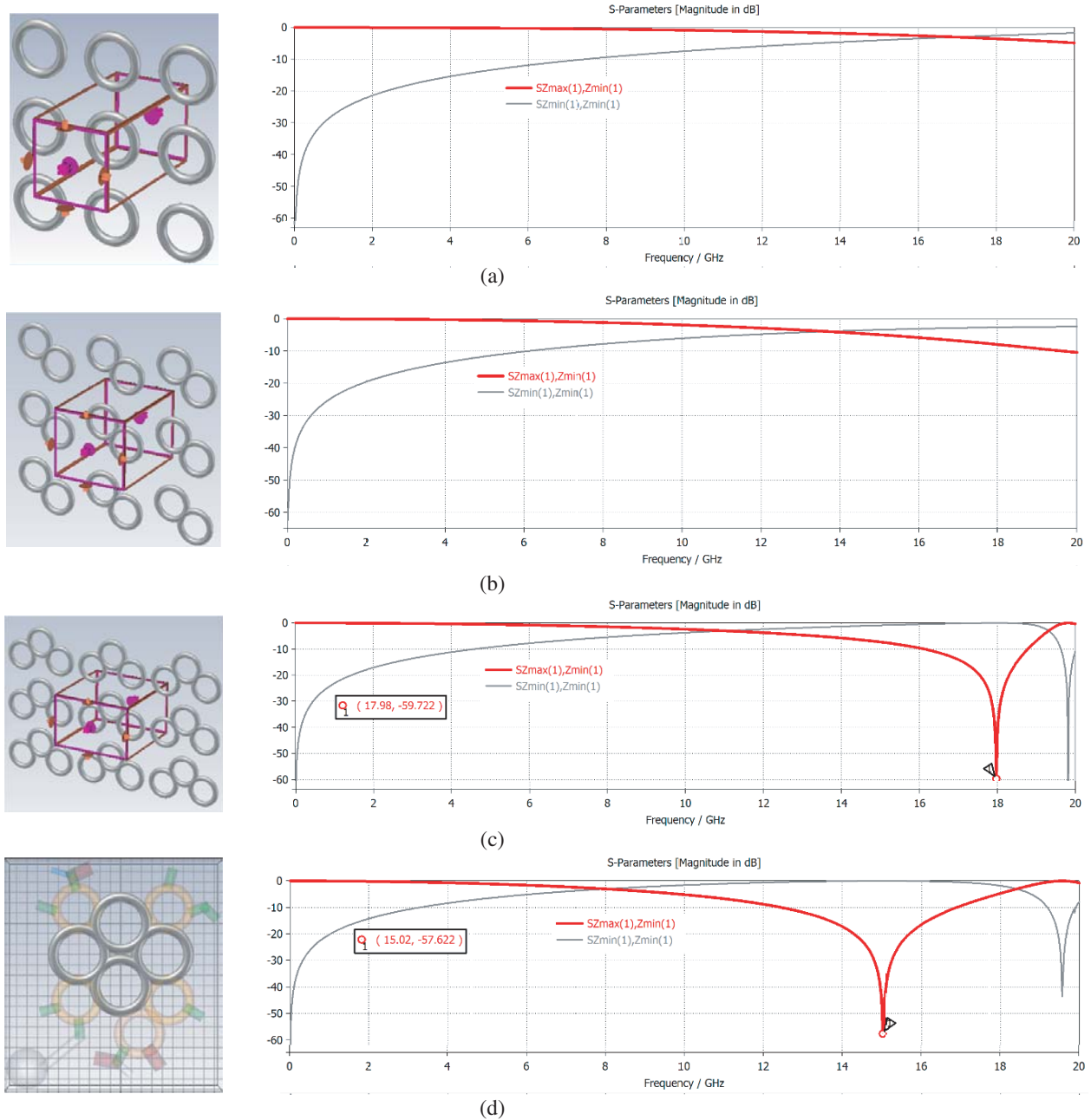
Figure 3. ChloroGreen 1st modelling steps: inner porphyrin ring, and their transmission properties.

structure. A closed ring in a torus shape, where the small and large radius were set at $2\,\mathrm{mm}$ and $3\,\mathrm{mm}$, respectively, was designed to represent one of the four rings in the inner loop of the porphyrin ring. All parts of this ChloroGreen metamaterial were built from perfect electric conductors (PEC). A full-wave excitation, operating from 0 to $20\,\mathrm{GHz}$ covering the X- and Ku-bands, was launched perpendicularly along the z axis to the ring plane. The periodic boundary was set so the structure was repeated in both axes, x and y, on the structure plane. All the simulations were performed using CST Microwave Studio software. As expected, all waves were transmitted with a slight absorption potential ($S_{21} \sim -5\,\mathrm{dB}$ at $20\,\mathrm{GHz}$) [11, 48–49]. The ChloroGreen 1st modelling step and transmission (S_{21}) and reflection (S_{11}) coefficients are presented in Figure 3(a). Another identical torus was placed at $45°$ adjacent to it, presented in Figure 3(b). The absorption level at the top of the observation frequency was more pronounced at $-10\,\mathrm{dB}$. The resonance ($-59.72\,\mathrm{dB}$) was first created at $17.89\,\mathrm{GHz}$ when three tori were combined (Figure 3(c)). Adding another torus to complete the inner loop of the porphyrin ring shown in Figure 3(d), increased the structure size; hence, the resonance ($-57.62\,\mathrm{dB}$) was shifted to a lower frequency at $15.02\,\mathrm{GHz}$.

A smaller torus, with the small and large radii of $1.5\,\mathrm{mm}$ and $2.5\,\mathrm{mm}$, or $1.5/2.5$ torus, was added on the top right of the inner porphyrin ring loop, presented in Figure 4(a). This extra torus broke the symmetry of the inner loop, resulting in another resonance at $16.38\,\mathrm{GHz}$ appearing next to the main resonance at $16.18\,\mathrm{GHz}$. Figure 4(b) shows the complete porphyrin ring where four identical $1.5/2.5$ tori were placed on four corners of the inner loop. This symmetric structure generated a single resonance at $17.6\,\mathrm{GHz}$. Then, in Figure 4(c) another $1.5/2.5$ torus was added at the bottom left of the porphyrin ring. It can be seen that there were multiple resonances (at $11.28\,\mathrm{GHz}$, $15.59\,\mathrm{GHz}$, $17.26\,\mathrm{GHz}$, and $19\,\mathrm{GHz}$) generated, due to the broken symmetry.
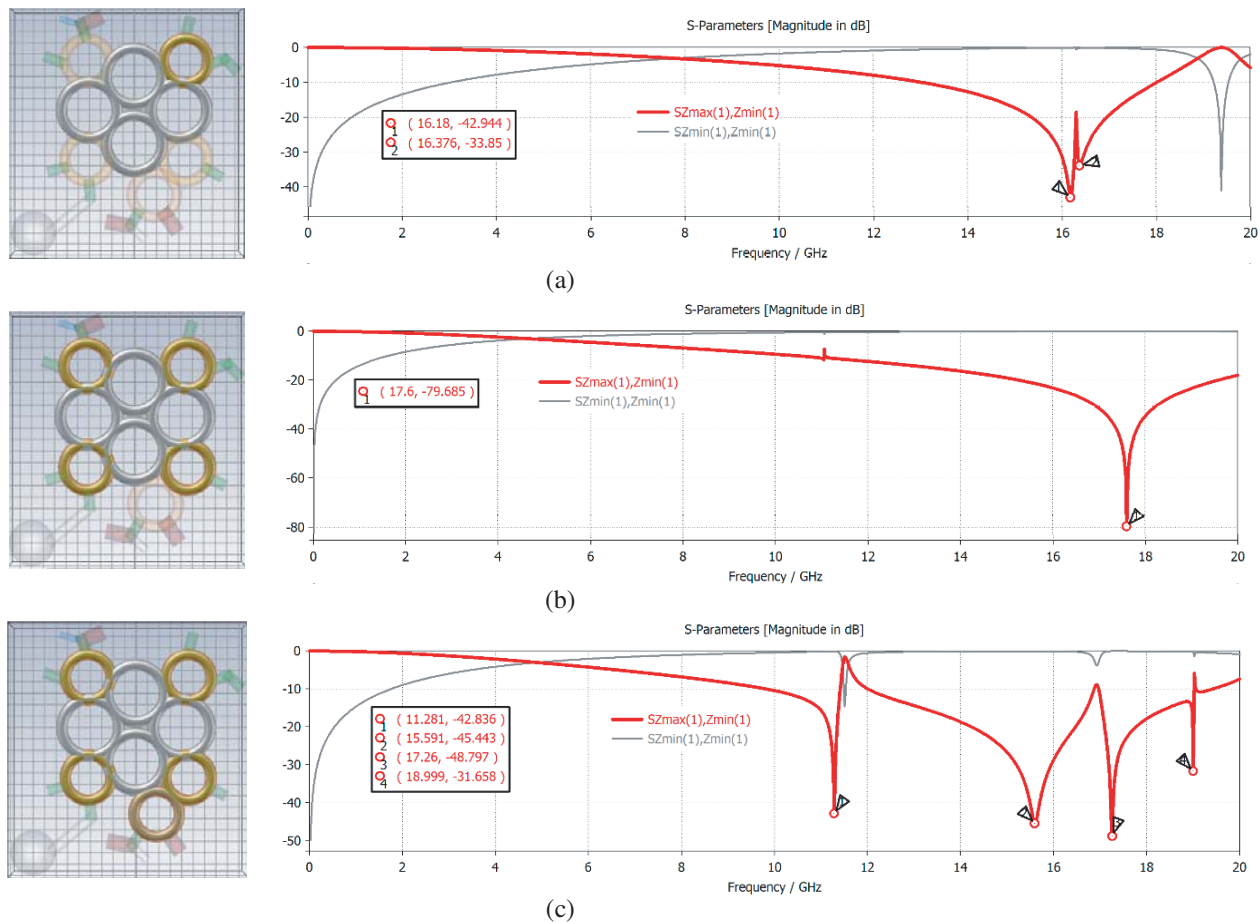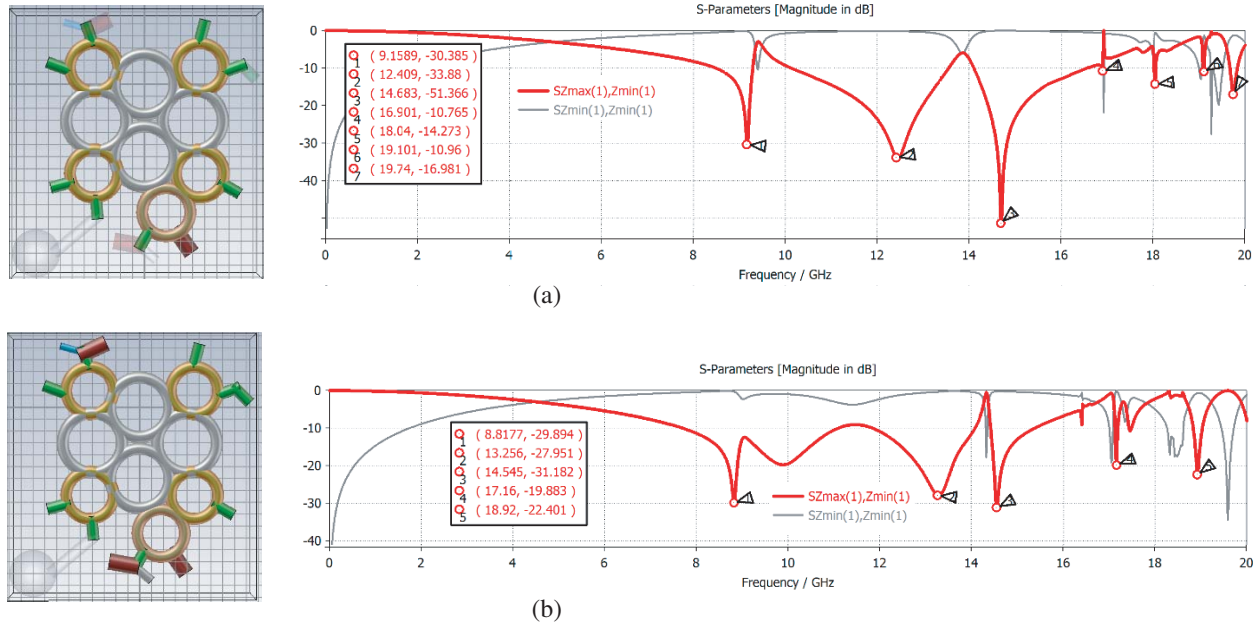

Figure 4. ChloroGreen 2nd modelling steps: porphyrin ring, and their transmission properties.

Nine short arms representing the bonding to the CH$_3$ and O-H molecules were added at the outer smaller five 1.5/2.5 tori, presented in Figure 5(a). There were more resonances occurring at higher frequency. Figure 5(b) presents the almost complete ChloroGreen structure where the second set of arms were connected to the first arm set. Here only the phytol tail was missing. It is interesting to note that these outer arms made the resonances broader. The transmission between the first two resonances was low, making the range in between (8.82 GHz–13.26 GHz) behave more like a broad absorption band.


Figure 5. ChloroGreen 3rd modelling steps: porphyrin ring with arms, and their transmission properties.

In the final modelling step, the artificial phytol tail was added to complete the ChloroGreen structure (Figure 6). There were ten resonances generated within the observed frequency range. The bandwidth of the first three resonances centered at 5.78 GHz, 8.90 GHz, and 11.72 GHz were significantly broad, indicating good absorbance.
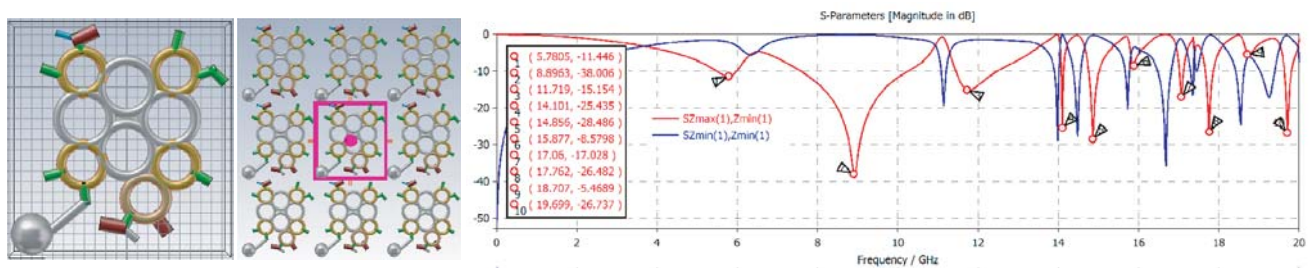
Figure 6. ChloroGreen metamaterial with their transmission properties.

The EM parameters, i.e., permeability, permittivity, and refractive index extracted from the S-parameters using the robust method [51], indicate the susceptibility and responses of the ChloroGreen to the EM waves within the operating wavelengths. The complex permeability and permittivity of the ChloroGreen are shown in Figures 7(a) and 7(b). The real part of the permeability was negative in the range of 8 GHz to 16 GHz. Within the aforementioned negative permeability range, there were five negative dips of the real part of the permittivity, marked at 11.02 GHz, 13.24 GHz, 14.14 GHz, 14.96 GHz, and 15.94 GHz. The overlapping of these negative values triggered the negative value of the
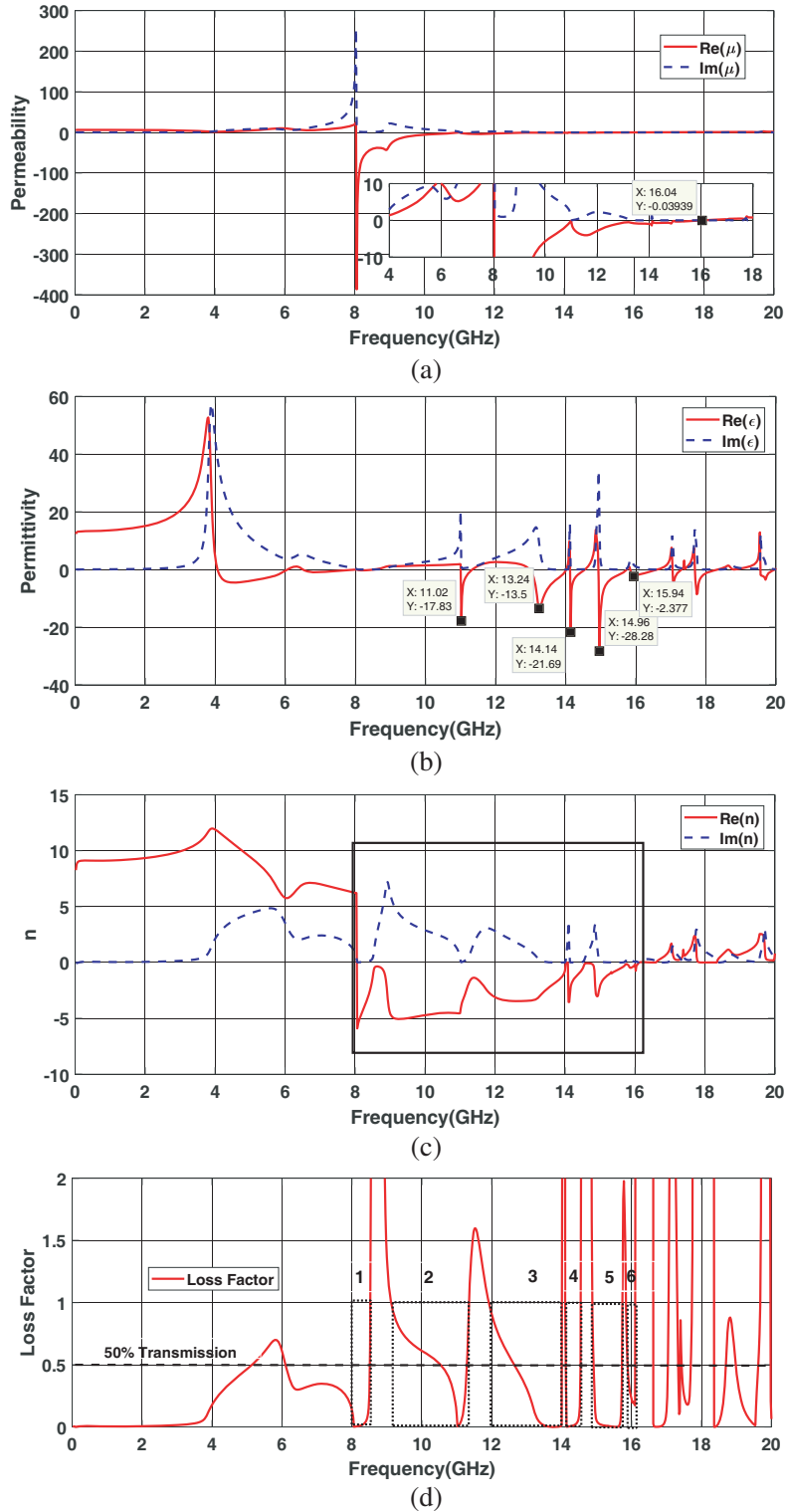
Figure 7. Complex (a) permittivity, (b) permeability, (c) refractive index and (d) the loss factor of the ChloroGreen.

refractive index, shown in Figure 7(c). To effectively simulate the NRI band, the complex values, both the real and the negative part, of permittivity and permeability must be taken into consideration [52–54].

As discussed earlier, the absorbance is a main function of Chlorophylls, and was established and also
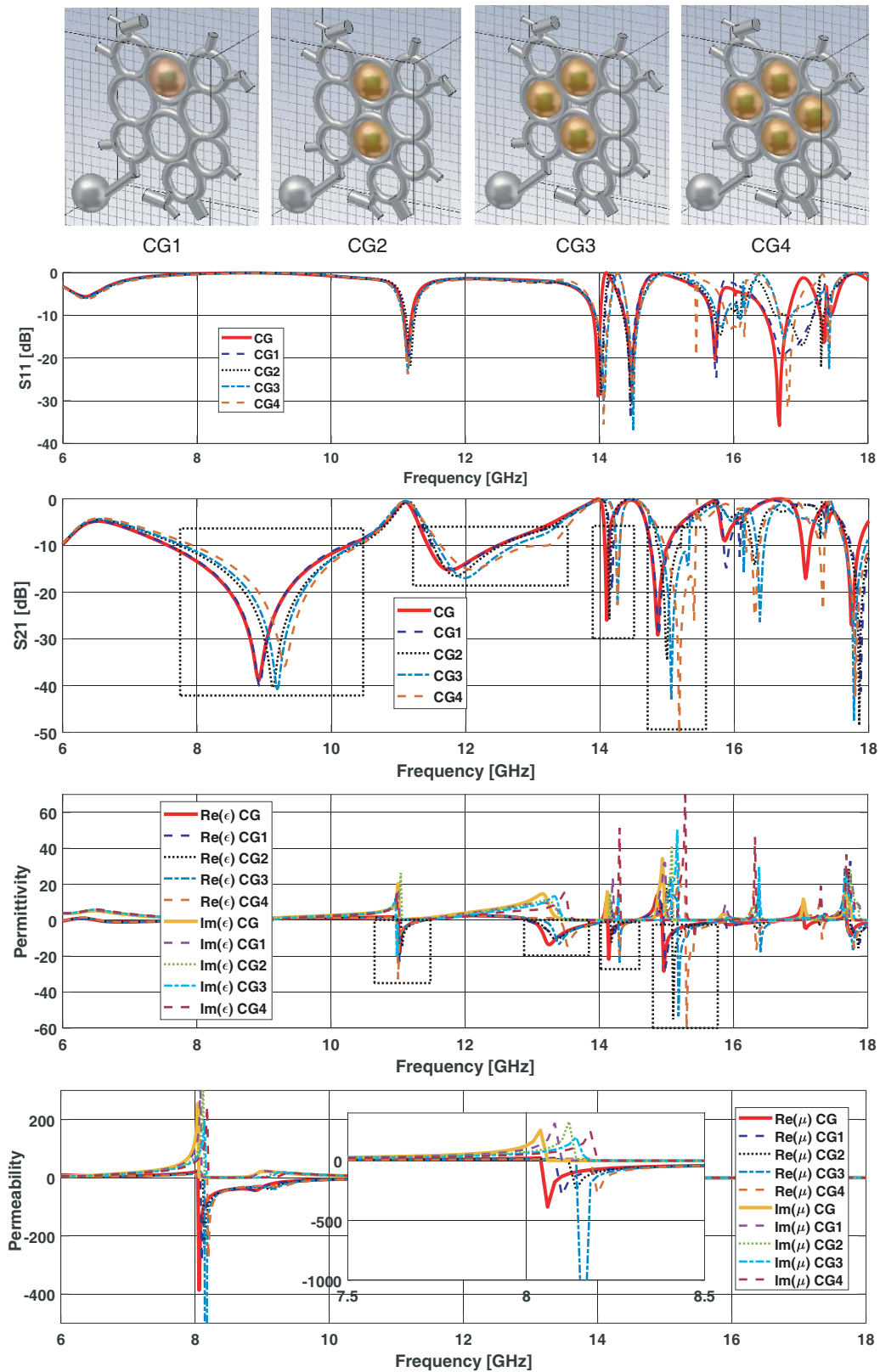
Figure 8. ChloroGreen — Modification 1: CG1, CG2, CG3 and CG4. (a) S_{11}, (b) S_{21}, (c) permittivity and (d) permeability.
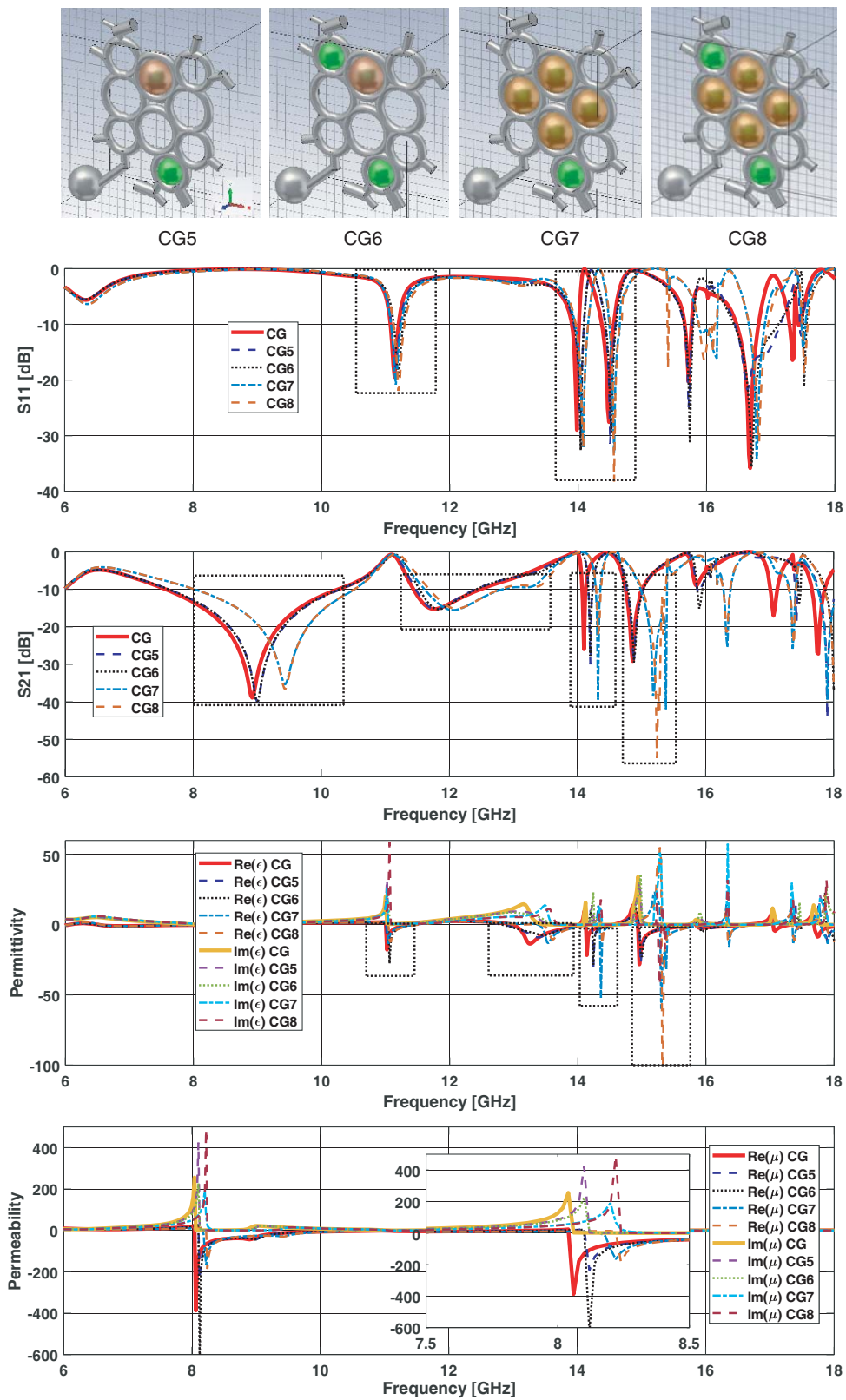
Figure 9. ChloroGreen — Modification 2: CG5, CG6, CG7 and CG8. (a) S_{11}, (b) S_{21}, (c) permittivity and (d) permeability.

Figure 10. ChloroGreen — Modification 3: CG, CG9, CG10, CG11 and CG12. (a) S_{11}, (b) S_{21}, (c) permittivity and (d) permeability.

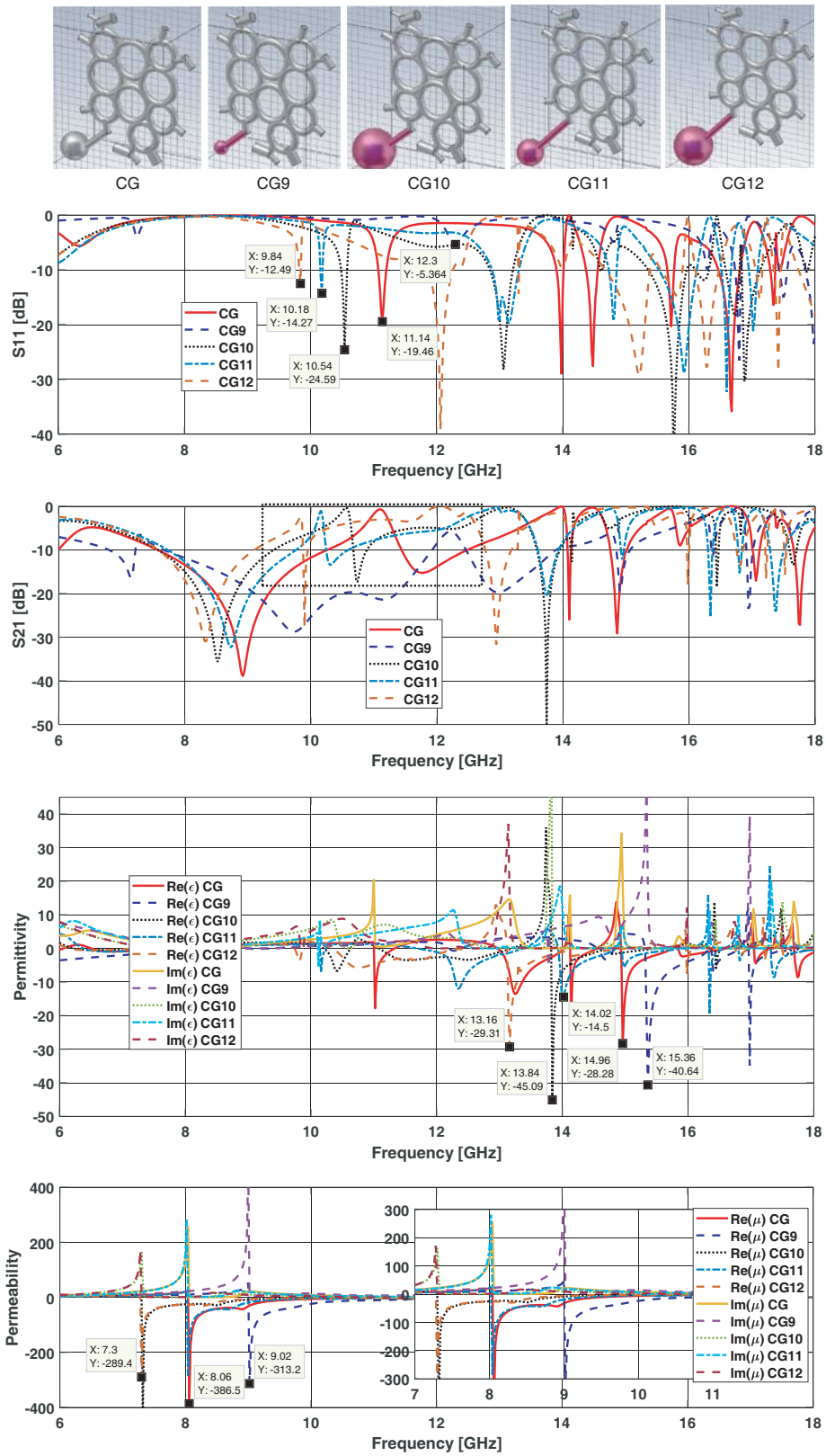confirmed in this ChloroGreen structure; however, focusing on the opposite point of view, this artificial structure can also generate a unique multiple (NIR) transmission bands between the absorption bands, that can benefit different EM and optics applications. The imaginary part of the refractive index, signifying material loss, both electrically and magnetically, is the main parameter used to calculate the loss factor or LF (LF $= \frac{\text{Img}(n)}{\text{Real}(n)}$) of the artificial materials [27–30, 54]. The LF of the ChloroGreen is plotted in Figure 7(c). There are six transmission bands surrounded by dotted boxes, where the LF of the ChloroGreen is less than one, representing the ranges, while the 0.5 level indicates 50% satisfactory transmission.

Following the modelling steps, there are several possibilities that can be heightened and further investigated in order to effectually manipulate the EM responses of the ChloroGreen. The first modification where spheres were added to fit inside the tori of the inner porphyrin ring demonstrated that the transmission and electromagnetic properties can be tuned. The resonances (S_{11} and S_{21}) were shifted to higher frequency as more spheres were added, resulting in the negative bands shift in both permittivity and permeability. The modified ChloroGreen structures and their EM responses are shown in Figure 8.

The smaller spheres were placed inside the outer porphyrin ring in the modification 2, presented in Figure 9. It can be seen that the results of adding both one and two spheres were similar if the core structure was the same, i.e., CG5 and CG6, and CG7 and CG8. The resonances and negative bands of CG7 and CG8 structures, where CG4 structure was used as the core structure, were higher.

Outstanding tuning results come from the adjustment of the artificial hydrophobic or phytol tail. Two cases of the hydrophobic tail adjustment were investigated: 1) the ball size: CG ($\Phi = 4$ mm), CG9 ($\Phi = 2$ mm) and CG10 ($\Phi = 6$ mm) and 2) the tail length: the tail length of CG11 ($\Phi = 4$ mm) and CG12 ($\Phi = 6$ mm) was double than those of CG, CG9 and CG10. Figure 10 presents the CG, and CG9-12 structures with the comparison of their transmission and EM properties. Considering the first group of the S_{11} resonances (dip location), also indicating the peak transmission (surrounded by the dotted rectangle), or the tips of the S_{21} parameter, the transmission tip of CG with a smaller ball was generated at the higher frequency, i.e., CG9 at 12.3 GHz, CG at 11.14 GHz, and CG10 at 10.54 GHz. The S_{11} resonances of the CG with longer tail were shifted to the lower frequency, i.e., CG11 at 10.18 GHz and CG12 at 9.84 GHz. The location of the negative permittivity dip (of the main group) of the CG with a smaller ball was also found at the higher frequency, i.e., CG9 at 15.36 GHz, CG at 14.96 GHz, and CG10 at 13.84 GHz. Similarly, the negative dip of those with a longer tail was located at the lower frequency (CG11 at 14.02 GHz and CG12 at 13.16 GHz). On the other hand, the permeability does not depend on the tail length. The negative permeability dips of CG and CG11, and CG10 and CG 12, were located at the same frequency at 8.03 GHz and 7.30 GHz, respectively. The negative dip of the smallest ball was created at the highest frequency at 9.02 GHz.

3. CONCLUSION AND DISCUSSION

The existence possibility of negative electromagnetic properties in Chlorophyll, i.e., permittivity, permeability, and refractive index, has been investigated. Design steps to create the bio-inspired metamaterials support the understanding of how these unique properties are generated, leading to effective property manipulation. The structures are designed in the microwave range and can be extended to the optical range. A very broad negative permeability band and five negative permittivity bands are found within the X- and Ku-bands from 8 GHz to 16 GHz, and can be effectively tuned by adjusting the structure and its orientation. These proposed Chlorophyll-inspired metamaterials are ready to be utilized or could be optimized for different usages.

ACKNOWLEDGMENT

REFERENCES

1. Fu, K., D. Moreno, M. Yang, and K. L. Wood, "Bio-inspired design: An overview investigating open questions from the broader field of design-by-analogy," *J. Mech. Des.*, Vol. 136, No. 11, 111102, 2014.

2. Hashemi, F. H. and U. Lindemann, *A Practical Guide to Bio-inspired Design*, Springer, 2019.

3. French, M., *Invention and Evolution: Design in Nature and Engineering*, Cambridge University Press, Cambridge, UK, 1988.

4. Benyus, J., *Biomimicry: Innovation Inspired by Nature*, Perennial, New York, 1997.

5. Blacklow, S. O., J. Li, B. R. Freedman, M. Zeidi, C. Chen, and D. J. Mooney, "Bioinspired mechanically active adhesive dressings to accelerate wound closure," *Science Advances*, Vol. 5, No. 7, 2019.

6. Cafferty, B. J., A. S. Ten, M. J. Fink, S. Morey, D. J. Preston, M. Mrksich, and G. M. Whitesides, "Storage of information using small organic molecules," *ACS Cent. Sci.*, Vol. 5, 911–916, 2019.

7. Shields IV, C. W., L. L. Wang, and M. A. Evans, "Materials for immunotherapy," *Adv. Materials*, 2019.

8. Silva-Candala, A. D., T. Brownb, V. Krishnanb, I. Lopez-Loureiroa, P. Ávila-Gómeza, A. Pusulurib, A. Pérez-Díazc, C. Correa-Paza, P. Hervellaa, J. Castilloa, S. Mitragotrib, and F. Camposa, "Shape effect in active targeting of nanoparticles to inflamed cerebral endothelium under static and flow conditions," *Journal of Controlled Release*, Vol. 309, 94–105, 2019.

9. Shi, N., C. C. Tsai, F. Camino, and G. Bernard, "Thermal physiology. Keeping cool: Enhanced optical reflection and radiative heat dissipation in saharan silver ants," *Science*, Vol. 349, No. 6245, 298–301, 2015.

10. Pendry, J. B., A. J. Holden, W. J. Stewart, and I. Youngs, "Extremely low frequency plasmons in metallic mesostructures," *Phys. Rev. Lett.*, Vol. 76, No. 25, 4773, 1996.

11. Pendry, J. B., A. J. Holden, D. J. Robbins, and W. J. Stewart, "Magnetism from conductors and enhanced nonlinear phenomena," *IEEE Trans. Microwave Theory Tech.*, Vol. 47, No. 11, 2075–2084, 1999.

12. Smith, D. R., J. B. Pendry, and M. Wiltshire, "Metamaterials and negative refractive index," *Science*, Vol. 305, No. 5685, 788–792, 2004.

13. Pendry, J. B., D. Schurig, and D. R. Smith, "Controlling electromagnetic fields," *Science*, Vol. 312, No. 5781, 1780–1782, 2006.

14. Wongkasem, N. and M. Ruiz, "Multi-negative index band metamaterial-inspired microfluidic sensors," *Progress In Electromagnetics Research C*, Vol. 94, 29–44, 2019.

15. Li, A., X. Zhao, G. Duan, and S. Anderson, "Diatom frustule-inspired metamaterial absorbers: The effect of hierarchical pattern arrays," *Adv. Functional Materials*, Vol. 29, No. 22, 2019.

16. Kim, T., J. Y. Bae, N. Lee, and H. H. Cho, "Metamaterials: Hierarchical Metamaterials for Multispectral Camouflage of Infrared and Microwaves," *Adv. Functional Materials*, Vol. 29, No. 10, 2019.

17. Krushynska, A. and F. Bosia, "Fractal and bio-inspired labyrinthine acoustic metamaterials," *Journal of the Acoustical Society of America*, Vol. 143, No. 1714, 2018.

18. Zhao, L. and S. Zhou, "Compact acoustic rainbow trapping in a bioinspired spiral array of graded locally resonant metamaterials," *Sensors*, Vol. 19, No. 4, 788, 2019.

19. Miniaci, M., A. Krushynska, A. S. Gliozzi, N. Kherraz, F. Bosia, and N. M. Pugno, "Design and fabrication of bioinspired hierarchical dissipative elastic metamaterials," *Phys. Rev. Applied*, Vol. 10, 024012, 2018.

20. Lakhtakia, A., D. E. Wolfe, M. W. Horn, J. Mazurowski, A. Burger, and P. P. Banerjee, "Bioinspired multicontrollable metasurfaces and metamaterials for terahertz applications," *Proc. SPIE, 10162, Bioinspiration, Biomimetics, and Bioreplication*, 101620V, April 17, 2017.

21. Zhao, Y., "Bio-inspired nanophotonics: Manipulating light at the nanoscale with plasmonic metamaterials," Ph.D. Dissertation, UT Austin, USA, 2013.

22. Matra, K. and N. Wongkasem, "Left-handed chiral isotropic metamaterials: Analysis and detailed numerical study," *J. Opt. A: Pure Appl. Opt.*, Vol. 11, 074011, 2009.

23. Panpradit, W., A. Sonsilphong, C. Soemphol, and N. Wongkasem, "High negative refractive index in chiral metamaterials," *J. Opt.*, Vol. 14, 075101, 2012.

24. Sonsilphong, A. and N. Wongkasem, "Three-dimensional artificial double helices with high negative refractive index," *J. Opt.*, Vol. 14, 105103, 2012.

25. Cui, Y., L. Kang, S. Lan, S. Rodrigues, and W. Cai, "Giant chiral optical response from a twisted-arc metamaterial," *Nano Lett.*, Vol. 14, No. 2, 1021–1025, 2014.

26. Zhou, J., D. R. Chowdhury, R. Zhao, A. K. Azad, H. Chen, C. M. Soukoulis, A. J. Taylor, and J. F. O'Hara, "Terahertz chiral metamaterials with giant and dynamically tunable optical activity," *Phys. Rev. B*, Vol. 86, No. 3, 035448, 2012.

27. Sonsilphong, A., P. Gutruf, W. Withayachumnankul, D. Abbott, M. Bhaskaran, S. Sriram, and N. Wongkasem, "Flexible bi-layer terahertz chiral metamaterials," *J. Opt.*, Vol. 17, 1–6, 2015.

28. Wongkasem, N., C. Kamtongdee, A. Akyurtlu, and K. Marx, "Artificial multiple helices: EM and polarization properties," *J. Opt.*, Vol. 12, 075102, 2010.

29. Sonsilphong, A. and N. Wongkasem, "Low loss circular birefringence in artificial triple helix," *Progress In Electromagnetics Research M*, Vol. 29, 267–278, 2013.

30. Sonsilphong, A. and N. Wongkasem, "Mid-infrared circular polarization switching in helical metamaterials," *J. Opt.*, Vol. 18, 115102, 2016.

31. Papadakis, G. T., D. Fleischman, A. Davoyan, P. Yeh, and H. A. Atwater, "Optical magnetism in planar metamaterial heterostructures," *Nature Communications*, Vol. 9, 296, 2018.

32. Zigoneanu, L., B. Popa, and S. A. Cummer, "Three-dimensional broadband omnidirectional acoustic ground cloak," *Nature Materials*, Vol. 13, 352–355, 2014.

33. Cummer, S. A., J. Christensen, and A. Alu, "Controlling sound with acoustic metamaterials," *Nature Reviews Materials*, Vol. 1, 16001, 2016.

34. Hou, X. and V. V. Silberschmidt, "Metamaterials with negative poisson's ratio: A review of mechanical properties and deformation mechanisms mechanics of advances materials," *Analysis of Properties and Performance*, 155–179, 2015.

35. Babaee, S., J. Shim, J. C. Weaver, E. R. Chen, N. Patel, and K. Bertoldi, "3D soft metamaterials with negative poisson's ratio," *Adv. Material*, 1–6, 2013.

36. Li, X., L. Gao, W. Zhou, Y. Wang, and Y. Lu, "Novel 2D metamaterials negative poisson's ratio and negative thermal expansion," *Extreme Mechanics Letters*, Vol. 30 100498, 2019.

37. https://hiscreation.com/node/1080 Accessed on December 13, 2019.

38. Wongkasem, N., "Identification of material parameters in complex metamaterials by group theory," *Technology and Innovation for Sustainable Development Conference*, (TISD 2008) Khon Kaen Thailand, 2008.

39. Mayer, J. R., "Die Organische Bewegung in ithren Zusammenhang mit dem Stoffwechserl," [The Organic Motion in its Relation to Metabolism], Heibronn:n.p., 1864.

40. Govindjee, E. R., *Photosynthesis*, Wiley, New York, 1969.

41. Whitmarsh, J. and E. R. Govindjee, "The photosynthetic process," https://www.life.illinois.edu/gov-indjee/paper/gov.html accessed on December 14, 2019.

42. Streitweiser and Heathcock, *Introduction to Organic Chemistry*, 2, MacMillan, New York, 1981.

43. Stryer, L., *Biochemistry*, W. H. Freeman and Co., San Francisco, 1975.

44. Moore, R., W. C. Dennis, K. R. Stern, and D. Vodopich, *Botany: Plant Diversity*, 1st Edition, Vol. 2, Wm. C. Brown, Dubuque, 1995.

45. Khan Academy Light and photosynthetic pigments, https://www.khanacademy.org/science/biology/photosynthesis-in-plants/the-light-dependent-reactions-of-photosynthesis/a/light-and-photosynth-etic-pigments, Accessed on December 14, 2019.

46. Arritt, B. J., D. R. Smith, and T. Khraishi, "Equivalent circuit analysis of metamaterial strain-dependent effective medium parameters," *J. of Applied Science*, Vol. 109, 073512, 2011.

47. Wongkasem, N., A. Akyurtlu, K. A. Marx, Q. Dong, J. Li, and W. D. Goodhue, "Development of chiral negative refractive index metamaterials for the terahertz frequency regime," *IEEE Trans. on Antennas and Propagation*, Vol. 55, No. 11, 3052–3062, 2007.

48. Wongkasem, N., A. Akyurtlu, J. Li, A. Tibolt, Z. Kang, and W. D. Goodhue, "Novel broadband THz negative refractive index metamaterials: Analysis and experiment," *Progress In Electromagnetics Research*, Vol. 64, 205–218, 2006.

49. Wongkasem, N., A. Akyurtlu, and K. A. Marx, "Group theory based design of isotropic negative refractive index metamaterials," *Progress In Electromagnetics Research*, Vol. 63, 295–310, 2006.

50. Katsarakis, N., T. Koschny, M. Kafesaki, E. N. Economou, and C. M. Soukoulis, "Electric coupling to the magnetic resonance of split ring resonators," *Appl. Phys. Lett.*, Vol. 84, No. 15, 2943–2945, 2004.

51. Chen, X., T. M. Grzegorczyk, B. I. Wu, J. Pacheco, Jr., and J. A. Kong, "Robust method to retrieve the constitutive effective parameters of metamaterials," *Phys. Rev. E*, Vol. 70, 016608, 2004.

52. Mackay, T. G., "Plane waves with negative phase velocity in isotropic chiral mediums," *Microw. Opt. Tech. Lett.*, Vol. 45, No. 2, 120–121, 2005.

53. Mackay, T. G. and A. Lakhtakia, "Simultaneous negative and positive phase-velocity propagation in an isotropic chiral medium," *Microw. Opt. Tech. Lett.*, Vol. 49, No. 6, 1245–1246, 2007.

54. Wongkasem, N. and A. Akyurtlu, "Light splitting effects in chiral metamaterials," *J. of Optics*, Vol. 12, 035101, 2010.